High-density arrays of x-ray microcalorimeters for Constellation-X

Caroline A. Kilbourne[a*], Simon R. Bandler[a,d], Ari D. Brown[a,e], James A. Chervenak[a], Enectali Figueroa-Feliciano[b], Fred M. Finkbeiner[a,f], Naoko Iyomoto[a,g], Richard L. Kelley[a], F. Scott Porter[a], Tarek Saab[c], John Sadleir[a,h], Jennifer White[a,i]

[a]NASA Goddard Space Flight Center, Greenbelt, MD 20771, USA
[b]Massachusetts Institute of Technology, Department of Physics, Cambridge, MA 02139, USA
[c]University of Florida, Department of Physics, Gainesville, FL 32611, USA
[d]University of Maryland, Department of Astronomy, College Park, MD 20742, USA
[e]NASA Postdoctoral Fellow with a guest researcher appointment at NASA Goddard Space Flight Center, Greenbelt, MD 20771, USA
[f]Science Systems and Applications, Inc., Lanham, Maryland 20706, USA
[g]Johns Hopkins University, Department of Physics and Astronomy, Baltimore, MD 21218, USA
[h]University of Illinois Physics Department, Urbana, IL 61801, USA
[i]Ohio State University, Physics Department, OH 43210, USA

ABSTRACT

We have been developing x-ray microcalorimeters for the Constellation-X mission. Devices based on superconducting transition-edge sensors (TES) have demonstrated the potential to meet the Constellation-X requirements for spectral resolution, speed, and array scale (> 1000 pixels) in a close-packed geometry.

In our part of the GSFC/NIST collaboration on this technology development, we have been concentrating on the fabrication of arrays of pixels suitable for the Constellation-X reference configuration. We have fabricated 8×8 arrays with 0.25-mm pixels arranged with 92% fill factor. The pixels are based on Mo/Au TES and Bi/Cu or Au/Bi absorbers. We have achieved a resolution of 4.0 eV FWHM at 6 keV in such devices, which meets the Constellation-X resolution requirement at 6 keV.

Studies of the thermal transport in our Bi/Cu absorbers have shown that, while there is room for improvement, for 0.25-mm pixels the standard absorber design is adequate to avoid unacceptable line-broadening from position dependence caused by thermal diffusion. In order to improve reproducibility and to push closer to the 2-eV goal at 6 keV, however, we are refining the design of the TES and the interface to the absorber. Recent efforts to introduce a barrier layer between the Bi and the Mo/Au to avoid variable interface chemistry and thus improve the reproducibility of device characteristics have thus far yielded unsatisfactory results. However, we have developed a new set of absorber designs with contacts to the TES engineered to allow contact only in regions that do not serve as the active thermometer. We have further constrained the design so that a low-resistance absorber will not electrically short the TES. It is with such a design that we have achieved 4.0 eV resolution at 6 keV.

Keywords: x-ray microcalorimeter, superconducting transition-edge sensor, imaging spectroscopy

1. INTRODUCTION

An x-ray microcalorimeter consists of at least three basic components: a high-quantum-efficiency material with low heat capacity to absorb the incident x-ray photons, a sensitive thermometer to register the resulting temperature change, and a thermal link to a low-temperature heat sink that sets the timing of the thermal recovery and the required bias

*Caroline.A.Kilbourne@nasa.gov

power in thermometers with Joule heating. If the assumption of instantaneous thermalization in the absorber is not valid, either because of diffusion times or non-thermal processes, then the link between the absorber and the thermometer becomes a fourth important component. Decoupling the absorber from the thermometer can be used to mask the effects of non-instantaneous thermalization, at the cost of thermal fluctuation noise from random energy exchange across that link. The energy-resolution penalty for a decoupled absorber increases with thermometer sensitivity and with the fraction of the device heat capacity that is in the absorber. Therefore, TES calorimeters are particularly sensitive to absorber decoupling because of their high α (logarithmic temperature sensitivity of the resistance, $d\log(R)/d\log(T)$) and the need to set the dynamic range via choice of heat capacity, most of which must reside outside of the sensor.

Because the absorber thermalization and the thermal conductance of the link between the absorber and the TES are such critical parameters, we have performed a series of measurements to determine both. The interpretation of the measurements has required sophisticated modeling of the detectors and of diffusion in the absorbers. The next section discusses the measurements and the models for our standard device design. In a subsequent section, we discuss our first results from some new device designs intended to improve both parameters.

2. BISMUTH/COPPER CANTILEVERED ABSORBERS

Our basic TES device, which has enabled resolution at 6 keV of as low as 4.4 eV full width at half maximum (FWHM), consists of a Mo/Au bilayer transition-edge thermometer with its superconducting transition temperature T_c near 0.1 K, a silicon nitride membrane to form an engineered thermal link to the heat sink, and a Bi/Cu x-ray absorber for high quantum efficiency over the astronomical x-ray band (up to ~ 12 keV). The membranes are defined by using deep reactive ion etching (DRIE) to etch straight from the back of a silicon wafer to the front-side nitride layer. We make

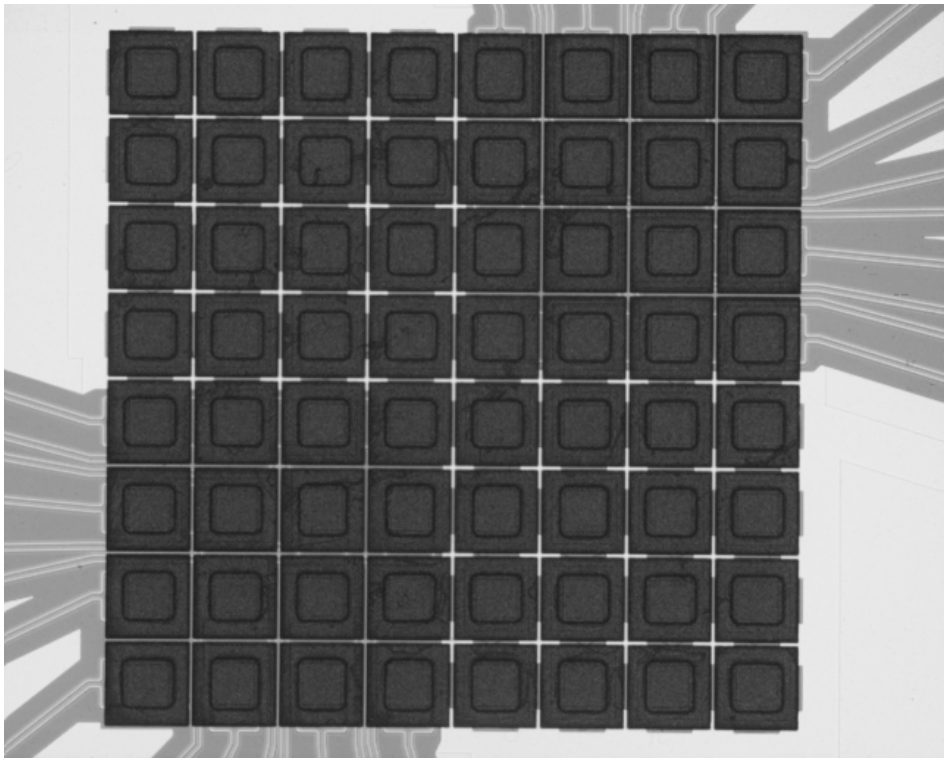

Fig. 1. 8×8 TES array with close-packed Bi/Cu absorbers on a 0.25-mm pitch. The contact between the absorber and the TES occurs only under the central square of each element; the remaining area of each absorber is a ledge that extends over the substrate without touching.

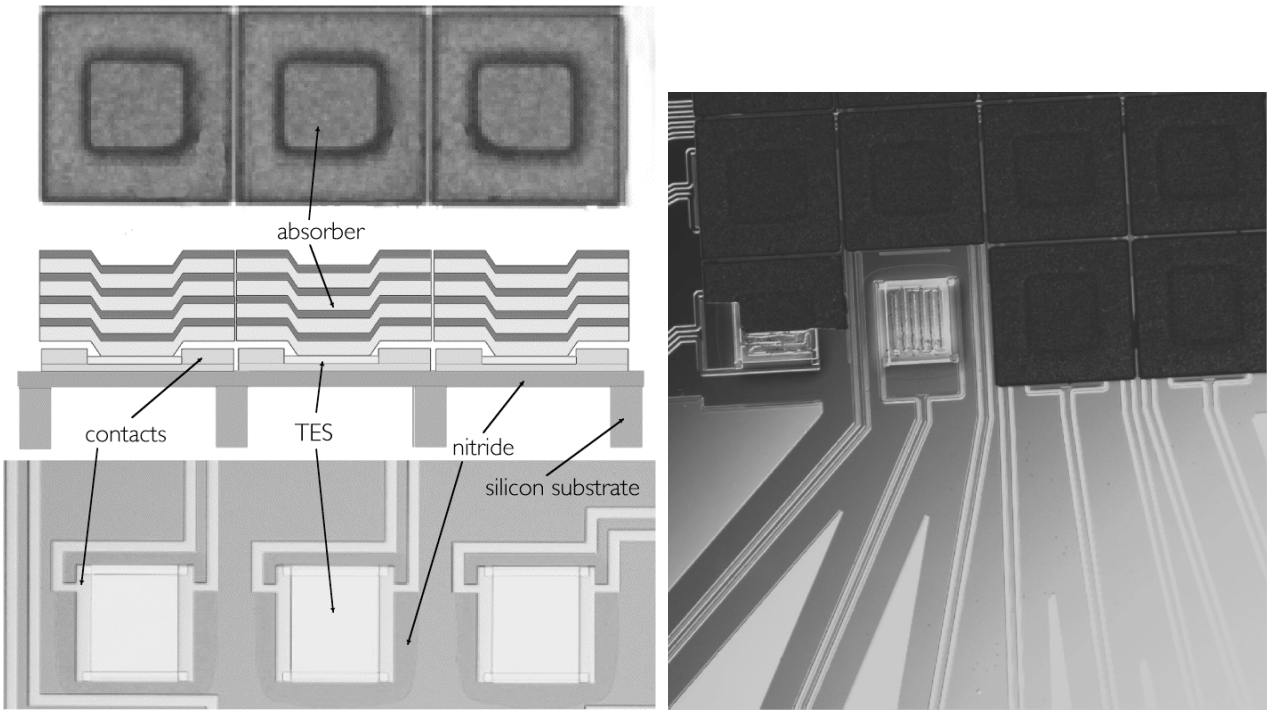

Fig. 2. *Left:* (from the top) face-on view of cantilevered "mushroom" absorbers, cross-sectional schematic showing an old absorber design with multiple layers, and face-on view of TES sensors without absorbers. *Right:* Portion of an 8×8 array with all of one absorber and a portion of another removed to show the underlying TES.

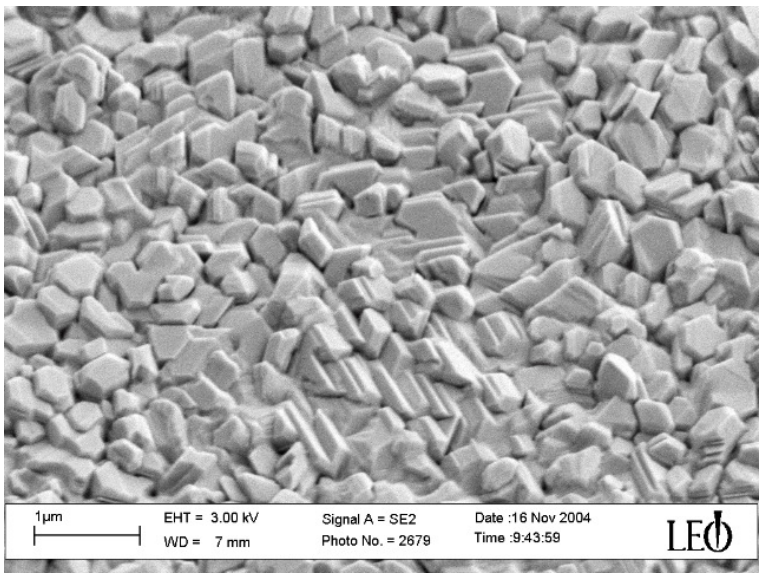

Fig. 3. Scanning electron micrograph of the grain structure of Bi deposited on Au.

Mo/Au bilayers in which the Mo and Au are electron-beam deposited under ultra-high vacuum (UHV) conditions. In order to design our devices for a particular heat capacity and x-ray opacity, we make our absorbers out of layers of Bi (low specific-heat semi-metal, high opacity) and Cu (high specific heat). Implicit in this design philosophy is the assumption that the Bi thermalizes the energy of the x-rays adequately, or that any shortfall in the ability of the Bi to thermalize is compensated by the Cu layers. Each Bi/Cu absorber contacts a TES in the middle and extends

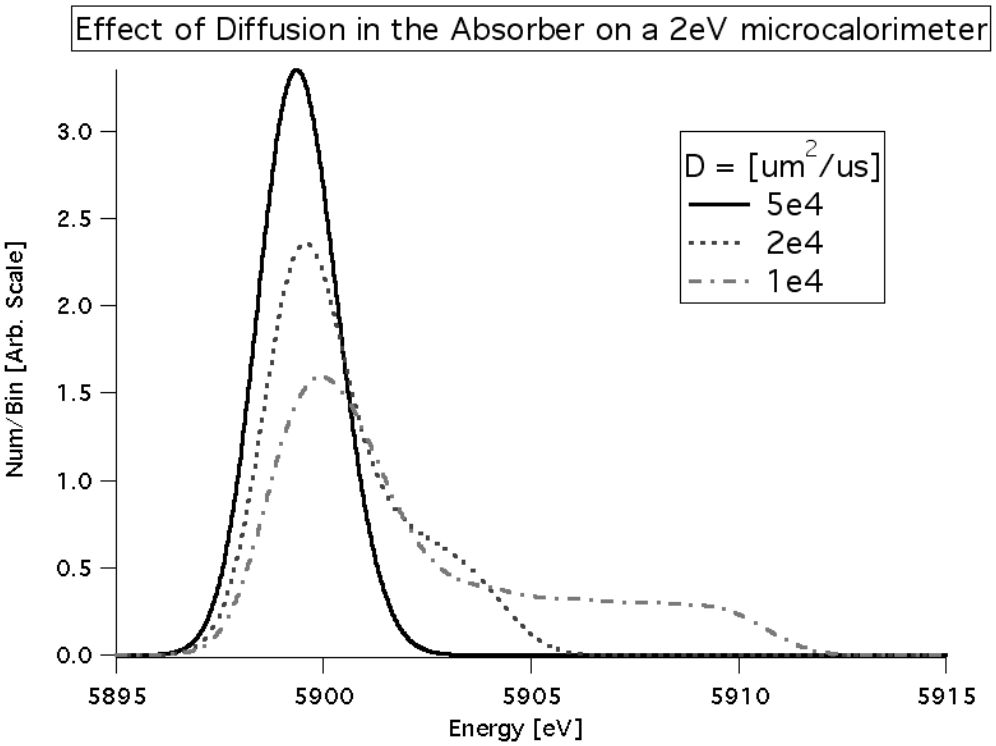

Fig. 4. Simulated line shape distortion resulting from absorbers with various diffusion constants for an absorber coupling of 1 μW/K.

cantilevered into the space around the TES, thus taking on a "mushroom" shape. The absorbers are produced by evaporating the metal layers into a double-layer photo-resist mold that defines both the contact areas and the separation of the absorbers; the actual separation is achieved via lift-off.[1] We produce 8×8 arrays with a 0.25-mm pitch. Figure 1 shows a standard 8×8 array and Figure 2 identifies its components. We have previously reported various physical characteristics of our Bi/Cu absorbers, both thermal[2] (thermal conductivity and diffusion constant) and chemical[3] (granularity and propensity for chemical diffusion and compound formation). Here we summarize the most important points that establish the foundation for subsequent discussion.

The electron density of Bi is sufficiently low that it does not alter the superconducting transition of the underlying Mo/Au bilayer (in the absence of chemical interaction). However, if Cu were in direct contact with the bilayer, its high electron density would suppress the T_c of the bilayer. Therefore, with our Bi/Cu absorbers it must be a Bi layer that is in direct contact with the TES. The 0.6-μm Cu thickness is set by the design heat capacity, and in our first absorbers we distributed the Cu among three or four equal layers within the 6.5-microns of Bi. We subsequently determined that our Bi grains were typically 0.2 μm in size (see Figure 3), and that using Cu layers of thickness comparable to the Bi granularity diminished the thermal conductance of the Cu layers. We also learned that Bi films thinner than 0.25 μm were smoother than thicker films even though they had roughly the same grain size. Therefore, we adopted an absorber design consisting of Bi/Cu/Bi with layer thicknesses of 0.1 μm, 0.6 μm, and 6.5 μm, respectively. Using a diffusion model to fit x-ray pulse data obtained from irradiating a long absorber strip between two TES sensors,[4] we have determined diffusion constants for this absorber configuration of $2 - 4 \times 10^4$ μm^2/μs.

We have recently assessed what diffusivity is required in a pixel suitable for the Constellation-X reference design. Due to the cantilevered nature of the absorber, the thermal path between the initial absorption point of the x-ray and the TES varies by as much as 70 μm. This effectively position-dependent thermal conductance between the absorber and the thermometer leads to variation in pulse rise times and an error in the determination of the deposited energy that increases linearly with energy. By numerically solving the diffusion equation for the geometry of the microcalorimeters,

we generated pulses for a grid of positions across the surface of the absorber and created a template pulse which was the mean of all the individual pulses. Using the template pulse and the theoretical noise response of the microcalorimeter to construct an optimal digital filter, we were able to determine the estimated energy as a function of position for the microcalorimeter.

Figure 4 shows the response of a microcalorimeter with 2 eV baseline resolution to a monochromatic 5.899 keV x-ray as a function of absorber diffusivity. In the model, we assumed an absorber-to-TES coupling of 1 μW/K, a value allowed by fits to the complex impedance[5] of some of our TES pixels and chosen because it does not significantly degrade the baseline resolution from that predicted for infinitely good absorber coupling. It can be seen that the detector response becomes non-Gaussian with a high-energy tail for values of diffusivity significantly below 5×10^4 $\mu m^2/\mu s$. The high-energy shoulder is due to the particular geometry of the absorber, namely, since the area in the cantilevered portion of the absorber is almost twice that of the contact area, the template pulse will be weighed towards the slower, smaller pulses of the cantilevered region. Events occurring over the contact area will have faster risetimes and larger pulse heights, causing the optimal filter to overestimate their energy. A weaker absorber coupling would degrade the baseline resolution, but would reduce the spread from diffusion.

3. MITIGATING INTERFACE CHEMISTRY

We fabricated a wafer of 8×8 arrays in the standard geometry just described (0.1/0.6/6.5-μm Bi/Cu/Bi atop a Mo/Au TES) that yielded multiple pixels with resolution at 6 keV of 4 – 5 eV FWHM. Materials analysis revealed no chemical interaction between the Bi and the underlying TES in devices from this wafer, while in some other fabrication runs we observed formation of BiAu intermetallics at the interface or diffusion of Cu through the Bi and into the Au of the TES.[3] The main problem with such interaction is that it alters the transition temperature of the Mo/Au bilayer from the value expected for the chosen Mo and Au thickness.

Because of the variable nature of the phenomenon, we investigated design modifications that would impede such interface reactions. Since the devices that resisted chemical interactions at the interface appeared to have an unknown and uncontrolled barrier layer, we investigated introducing a barrier layer of another material. We assessed basic materials compatibility as well as integrability into our absorber fabrication process. Since detector properties (normal resistance, T_c) are affected by thick metal layers while insulators can affect thermalization of absorber to detector, we examined possible thin barrier layers of metals and insulators that can be readily patterned to insert between the Bi and Au layers in the device. Tests of thin Ge and Mo layers showed excellent compatibility with Bi at elevated temperatures (>120 °C), but at similar temperatures (required for processing of the absorber), the Ge diffused into the Au films. The Mo/Au interface, however, is stable at these temperatures (indeed this motivated our selection of Mo/Au for the TES bilayer). A heated substrate is required for electron-beam deposited Mo to have a superconducting transition temperature approaching that of bulk Mo; when deposited on a cold substrate, it usually remains normal conducting to below 50 mK. In experiments thus far with using a capping Mo layer between the TES and the Bi, we have found the impact of this normal-conducting Mo film on the T_c of the underlying bilayer to be too variable to incorporate it into our process as a barrier layer at this time.

Other metals, such as Ti and Cr also interact with the Au at or below our processing temperature. Sputtered W is a promising candidate but sputtering alters our current fabrication procedure and we have yet to test it. Pt can be deposited with electron-beam evaporation but is expected to affect the device when its thickness is sufficient to provide a barrier. Insulators such as a-Si (sputtered), SiO (liquid-phase chemical vapor deposition) and AlO (electron-beam) are all candidates for readily deposited barrier layers. In general, insulators are advantageous because they would allow arbitrary arrangement of the materials in the absorber (e.g. thick thermalizing metal on the bottom) and arbitrary geometry of the absorber. However, insulators can have high heat capacities and require additional materials (e.g. Ti) to provide an adhesion layer for other metal films. Also, additional patterning of the absorber may be required to create regions of metallic contact between the detector and absorber thermalization layer. Otherwise, the electron systems of the absorber and TES would be connected only via phonons, and thus could be slow. Investigations of these other metal and insulator candidates will be a part of our future work.

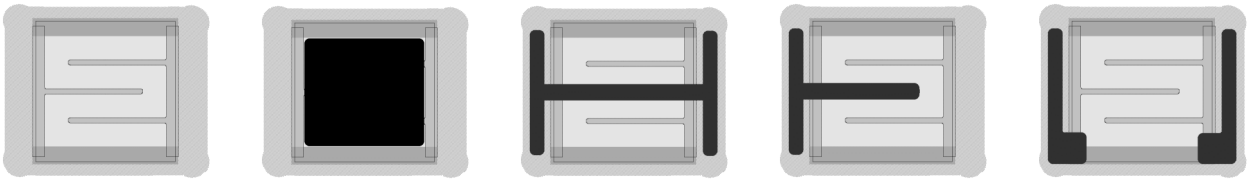

a b c d e

Fig. 5. Absorber contact with TES or membrane shown in black. a: unobscured TES, showing noise mitigating, normal-metal stripes, superconducting contacts, and nitride membrane around the square of the device. The current flows from top to bottom, b: contact area of conventional absorber, c, d, e: variations of the new design, showing how contact to the active areas of the TES is limited and how supports are contrived to avoid electrically shunting the sensor with the absorber.

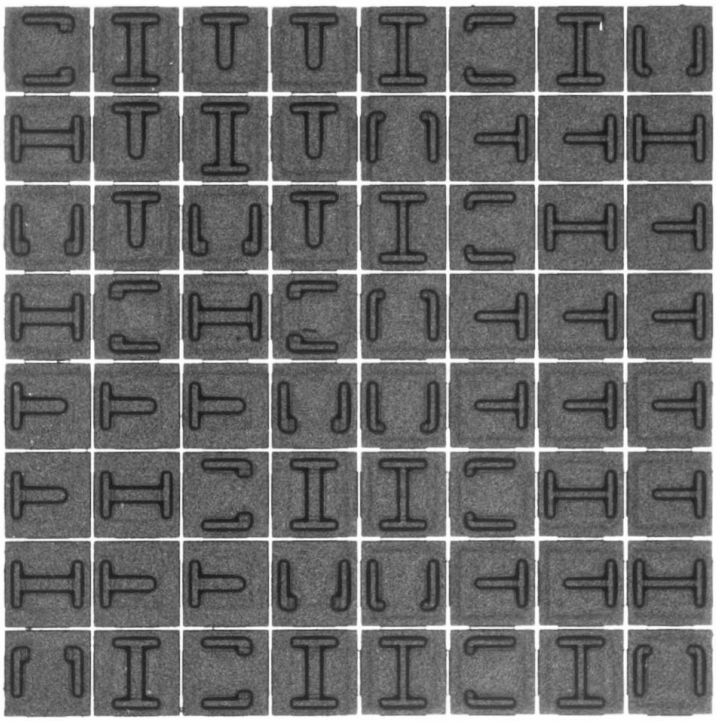

Fig. 6. 8x8 array for testing variations of the geometry of the absorber contact area. The outlined shapes are in contact with the TES or the membrane, the other areas of the absorber are freestanding.

As an alternative to a chemical barrier, we investigated introducing a vacuum gap between the absorber and the TES. We have designed absorbers that are cantilevered over the active part of the TES itself, making contact only at normal metal features. Each TES has normal conducting regions within and alongside the active thermometer. Banks of thick Au on the edges parallel to the current flow define the superconducting boundary condition and make the transition shape more uniform than if the superconducting boundary were etch-defined. Interdigitated stripes of thicker Au distributed within the TES perpendicular to the current flow have been shown by our group and others to mitigate excess white noise.[6] These regions are available for making good thermal contact between the TES and absorber without changing the properties of the TES.

We also wish to avoid a geometry that places a low-resistance absorber in parallel with the TES. The normal-state resistance of our TES devices is 8 – 10 mΩ, and they are typically operated at a resistance of a few mΩ. The resistance of the bottom Bi layer in our standard absorber was sufficiently high that it did allow the absorber to shunt current from the TES, but improving the electron transport in such an absorber to accelerate thermalization could also render it an

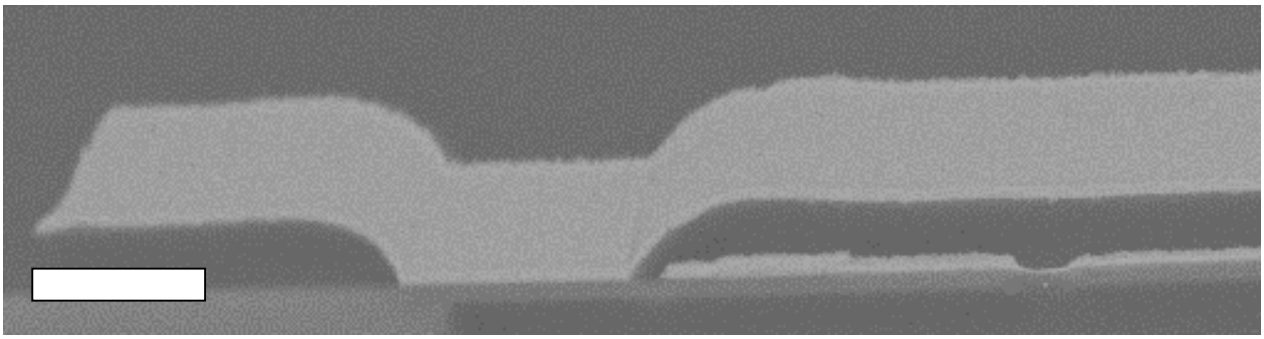

Fig. 7. Electron micrograph of a cross-section of a Au/Bi absorber, showing the absorber extending over the substrate on the left and over the TES on the right. Scale bar = 10 μm.

electrical shunt that would diminish the sensitivity of the device. We therefore designed the absorber contacts not only to avoid the active region of the TES, but also to avoid contact that would provide a parallel current path through the absorber. In order to provide adequate mechanical support for the cantilevered absorber, the new absorber designs include contacts to the membrane outside of the normal-metal edges of the TES. Figure 5 shows schematic representations of several designs for the contacts that are under investigation. In each, the solid black filled shapes represent the only area in which the absorber is in contact with the TES or the adjacent membrane; elsewhere it is cantilevered above them. The conventional design is also shown for reference. The square of the TES is 0.14 mm wide, whereas the full absorber structure is 0.24 mm wide. The hash marks show the extent of the nitride membrane. The details of the normal-conducting features and superconducting contacts can be seen, but the electrical leads are not shown in these drawings.

4. GOLD/BISMUTH ABSORBERS

In our first tests of the new absorber design, we have already taken advantage of the non-shunting aspect and have made absorbers consisting of a bottom 0.7-μm layer of Au followed by a 6.5-μm layer of Bi. Figure 6 shows one of the 8×8 arrays with the range of absorber contact tests, and Figure 7 is an electron micrograph of a cross-sectioned absorber. Preliminary measurements indicate the diffusivity in these absorbers is a factor of 2 higher than in the Bi/Cu/Bi absorbers.

Due to an alignment error, many devices were shorted and could not be tested. However, we have achieved 4.0 – 4.5 eV resolution FWHM at 6 keV in three pixels – two of the "T" design and one of the "H" design. We have not yet completed characterization of the thermal parameters of the device, but there are several promising indications. A distinct population of faster rising events due to x-ray absorption directly in the TES could not be found, even though we have routinely identified such a population for the Bi/Cu/Bi absorbers. The thermal conductance of the membrane was measured to be 1.9×10^{-10} W/K (referred to 0.1 K) for both the T and H design, similar to what we have measured previously for 0.5-μm nitride membranes and our conventional design. Thus the scaling of thermal conductivity with the perimeter of the device[7] breaks down when the perimeter folds back upon itself, as we expected.

Figure 8 is a spectrum from ^{55}Fe showing the 4.0-eV resolution of one of the T devices. We are still working to identify the origin of the shoulder on the low energy side of the lines. We did not see such a low-energy shoulder on lines measured with good conventional absorbers. This feature is the same in the response of both the H and T design, which eliminates energy loss via the direct contact of the absorber with the nitride as an explanation. Applying the diffusion model to these geometries ought to be illuminating.

5. ELECTROPLATED GOLD ABSORBERS

The next step in improving absorber thermalization and minimizing the effects of interface chemistry is to work with a solid Au absorber. We have investigated the feasibility of electroplating a 4-μm thick Au absorber into the new absorber

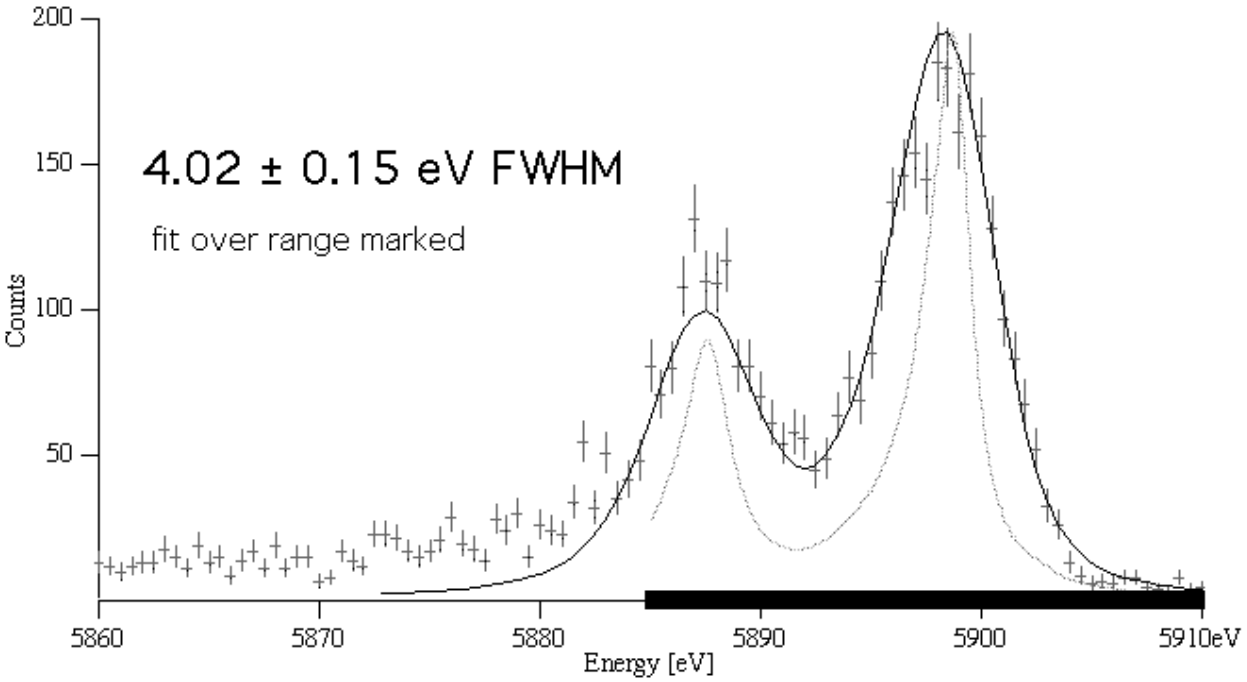

Fig. 8. Spectrum from ^{55}Fe showing the 4.0-eV resolution and low-energy shoulder of the response of one of the Au/Bi devices with a T-shaped absorber contact.

geometry. Such a device will have a quantum efficiency of 97% at 6 keV, but will have roughly four times the heat capacity of our Bi/Cu or Bi/Au absorbers at the same operating temperature. The design of a TES, however, requires matching heat capacity with the right value for α, while also optimizing for linearity, noise, and other non-ideal effects. Studying thermalization in these simple absorbers will aid in interpreting the response of TES's with more complex absorbers and will contribute to the overall optimization of the design.

To this end, we have conducted a set of initial electroplating runs in which we have integrated electroplated Au absorbers into our TES design. The absorber fabrication is identical to the process outlined in the preceding section with the exception that the evaporated 0.7-μm Au and 6.5-μm Bi layers are substituted with a 0.2 μm electron-beam evaporated Au seed layer and 4 – 5 μm of electroplated Au. We have not yet tested these devices; however, we have measured the 4.2-Kelvin resistivity and residual resistivity ratio (RRR, the ratio of the 300-K to 4.2-K resistances) of these samples to equal 4.8 – 6.5 $\times 10^{-10}$ Ωm and 36 – 45, respectively. These values compare favorably with the 4.2-K resistivity and RRR of bulk gold (2.2×10^{-10} Ωm and 103, respectively[8]), and consequently the thermal conductance of these electroplated absorbers should be high.

6. ASSESSMENT TO-DATE AND FUTURE WORK

We have made considerable progress with the design of compact TES arrays suitable for Constellation-X, improving the resolution to 4 eV FWHM at 6 keV while removing a chemically vulnerable interface from the design. Future work with this new design includes testing the electroplated Au absorbers and other ratios of Au and Bi (and perhaps Cu again) in order to identify the origin of the low-energy shoulder of the line response.

The design of absorber contact supports on the membrane outside of the TES increases the required membrane area, shrinking the width of the thick silicon frame that lies between pixels. This substrate is used to support wiring on the top and, ultimately, a backside Au layer for heatsinking the array. Optimization of the vacuum-gap absorbers will ultimately require using a smaller TES so that the membrane can be reduced to its former size.

As discussed in Section 3, we plan to investigate other options for insulating and metallic barrier layers that can be put in place between the absorber and TES in the conventional absorber scheme. Our studies thus far of Ge and Mo were by no means exhaustive. Use of an insulating layer, like the vacuum-gap approach, would permit high-conductivity absorbers, yet would minimize the area of cantilevered absorber and eliminate the need for contact on the membrane. This may combine the best of the conventional and the new design. It may not be necessary to open areas of the insulator to allow direct contact of the absorber with metallic features of the TES. As long as electron-phonon coupling is adequate on both sides of the insulator, the loss of a direct electronic connection will not be detrimental.

ACKNOWLEDGMENTS

We are grateful to Kent Irwin and his research group at NIST – Boulder for many valuable discussions and for providing NIST SQUIDs and NIST multiplexer components and electronics. We are similarly grateful to Jörn Beyer of PTB – Berlin for valuable discussions and for providing the PTB SQUID arrays that we have used for some of our measurements. This research was supported in part by an appointment (A. Brown) to the NASA Postdoctoral Program at NASA Goddard Space Flight Center administered by Oak Ridge Associated Universities through a contract with NASA.

REFERENCES

1. N. Tralshawala, et al., "Design and fabrication of superconducting transition edge X-ray calorimeters", *Nucl. Inst. and Meth. A*, 444(1-2), 188-191 (2000).
2. N. Iyomoto, et al., "Optimization of X-ray absorbers for TES microcalorimeters", *Proc. SPIE* 5501, 145-154 (2004).
3. J. E. Sadleir, et al., "Bismuth X-ray Absorber Studies for TES Microcalorimeters", *Nucl. Inst. and Meth. A* 559(2), 447-449 (2006).
4. T. Saab, et al., "Determination of lateral diffusivity in single pixel X-ray absorbers with implications for position dependent excess broadening", *Nucl. Inst. and Meth. A* 559(2), 447-449 (2006).
5. T. Saab, et al., "Determination of complex microcalorimeter parameters with impedance measurements", *Nucl. Inst. and Meth. A* 559(2), 712-714 (2006).
6. M. A. Lindeman, et al., "Characterization and reduction of noise in Mo/Au transition edge sensors", *Nucl. Inst. and Meth. A* 520(1-3), 426-428 (2004).
7. C. K. Stahle, et al., "Arraying Compact Pixels of Transition-edge Microcalorimeters for Imaging X-ray Spectroscopy", *AIP Conf. Proc*. 605, 223-226 (2001).
8. D. R. Lide, "Handbook of Chemistry and Physics 75th Ed." New York: CRC Press, 1996-1997: 11-41.